J Mater Sci (2017) 52:1573–1580

The electrochemical properties of one-pot prepared Fe_2SSe/porous carbon composite as anode material for lithium-ion batteries

Jia-Chuang Li[1], Ze Ma[1], Yang Chi[1], and Sheng-Ping Guo[1,2,*]

[1] College of Chemistry and Chemical Engineering, Yangzhou University, Yangzhou 225002, Jiangsu, People's Republic of China
[2] State Key Laboratory of Structural Chemistry, Chinese Academy of Sciences, Fujian Institute of Research on the Structure of Matter, Fuzhou 350002, Fujian, People's Republic of China

Received: 13 July 2016
Accepted: 27 September 2016
Published online: 4 October 2016

© Springer Science+Business Media New York 2016

ABSTRACT

The Fe_2SSe particles dispersed in the pores of carbon (Fe_2SSe/PC) were prepared using a simple one-pot solid-state method, which were then characterized by XRD, SEM, TEM, XPS, and Raman spectrum techniques. As the anode material for lithium-ion batteries, Fe_2SSe/PC displays an initial discharge capacity as high as 699.5 mAh/g at 0.1 C, and 327.9 mAh/g can be maintained after 200 cycles, much enhanced than those of pure Fe_2SSe. The small particles of Fe_2SSe wrapped in carbon can effectively buffer the volume expansion during charging/discharging to improve the electrochemical performance.

Introduction

Lithium-ion batteries (LIBs) are playing a more and more significant role in energy storage along with the rapid development and requirement of high-power current-consuming equipments [1–8]. As an important component of LIBs, the anode material makes great contribution to its capacity and influences the whole electrochemical performance of LIBs. The commercial graphite has been widely used as anode materials for LIBs because of its excellent cycling stability [9–11]. However, its low theoretical capacity (372 mAh/g) cannot meet the requirement of LIBs with high energy density and power density. So, it is continuously meaningful to explore novel anode materials.

As anode material for LIBs, ferrous sulfide (Fe S) has attracted much attention to be extensively studied [12–18] because of its high theoretical capacity (609 mAh/g) and the low cost of iron. However, the cycling stability of FeS is poor due to the large volume expansion during charge and discharge. Relatively, ferrous selenide (FeSe, theoretical capacity:397 mAh/g) has a better cycling stability and higher conductivity than FeS [19–22]. So, a double-anions compound, Fe_2SSe, was designed and prepared. Fe_2SSe combines the advantages of FeS and FeSe, and it has a higher theoretical capacity (480 mAh/g) and operating voltage (ca. 1.4 V vs. Li^+/Li) than that of graphite (below 0.2 V vs. Li^+/Li). J. B. Liu et al. prepared Fe_2SSe using ball-milling method followed by sintering, and the as-prepared

Address correspondence to E-mail: spguo@yzu.edu.cn

DOI 10.1007/s10853-016-0451-1

Fe_2SSe could deliver an initial discharge capacity of 471 and 397.2 mAh/g could be remained after 100 cycles at 0.1 C [23]. So far, this is the only study of Fe_2SSe as anode material for LIBs. Differently, one-pot solid-state method was employed to prepare Fe_2SSe/PC composite here, which can be simply described as the synthesis of Fe_2SSe and PAN carbonization finished at the same time in one reactive system. This method should be introduced to prepare other types of metal chalcogenides/carbon composites. It is necessary to investigate Fe_2SSe much more to get better understanding and try to enhance its electrochemical performance.

In our work, the Fe_2SSe particles wrapped in carbon using a simple one-pot solid-state method, namely, Fe_2SSe/PC, exhibit a first discharge capacity of 699.5 mAh/g at 0.1 C and 327.9 mAh/g can be left after 200 cycles.

Experimental

Preparations and material characterizations

The Fe_2SSe/PC was prepared by heating Fe (99 %, aladdin), Se (99.9 %, aladdin), S (99.95 %, aladdin), and PAN (M_w 150000, Sigma-Aldrich) mixed with the molar ratios of 3:2 for (Fe, Se, S):PAN and 2:1:1 for Fe:Se:S in an evacuated quartz tube. The quartz tube was firstly heated from room temperature to 400 °C with the speed of 0.5 °C/min and homogenized at 400 °C for 5 h. Then the temperature was heated at 900 °C with the same heating rate and maintained for 10 h. Finally, the black sample was obtained through natural cooling to room temperature. In addition, pure Fe_2SSe and carbonized PAN were prepared using the same method.

Powder X-ray diffraction (PXRD, Bruker D8 Advance) analysis was performed at 40 kV and 100 mA for Cu-$K\alpha$ radiation ($\lambda = 1.5406$ Å) with a scan speed of 5 °/min at room temperature. Energy-dispersive X-ray spectroscopy (EDS, Bruker, Quantax) was used to analysis the element content. Energy-dispersive X-ray spectroscopy element mapping was employed to show the distributions of Fe, S, Se, and C in Fe_2SSe/PC. Scanning electron microscopy (SEM, Supra 55 Sapphire) and transmission electron microscopy (TEM, Philips Tecnai12) were used to observe the surface morphology and size. Raman spectrum (Renishaw in via) and X-ray photoelectron spectroscopy (XPS, Thermofisher Scientific, ESCALAB250Xi) were used to analyze the chemical structures and chemical composition, respectively.

Electrochemical measurements

The electrodes were composed of 80 wt% active material (Fe_2SSe/PC or Fe_2SSe), 10 wt% carbon black, and 10 wt% polyvinylidene fluoride (PVDF), respectively. The slurry was prepared by stirring the mixture in a certain amount of *N*-methyl-2-pyrrolidinone (NMP), then coated the slurry onto a copper foil. After dried at 120 °C for 12 h in a vacuum oven, the foil was cut into disks with diameter of 1.6 cm.

The CR-2032-type coin cells were assembled using a Li foil as the counter electrode and a Celgard 2325 film as the separator in a glovebox (VAC-Omni 102283) filled with argon, where oxygen and water contents were less than 1 ppm. The electrolyte was 1 M $LiPF_6$ in 1:1 DEC/EC. Cyclic voltammetry (*C*–*V*) measurements were carried out on an electrochemical workstation (CHI660D) in 1.0–3.5 V with a scan rate of 0.1 mV/s. Electrochemical impedance spectroscopies (EIS) were measured over a frequency range of 0.01 Hz–100 kHz. The galvanostatic charge/discharge tests were carried out at 0.1 C (48 mAh/g) in the voltage range of 1.0–3.5 V using NEWARE CT-3008 battery charge–discharge system. The charge–discharge data were recorded after the first discharge to 1.0 V.

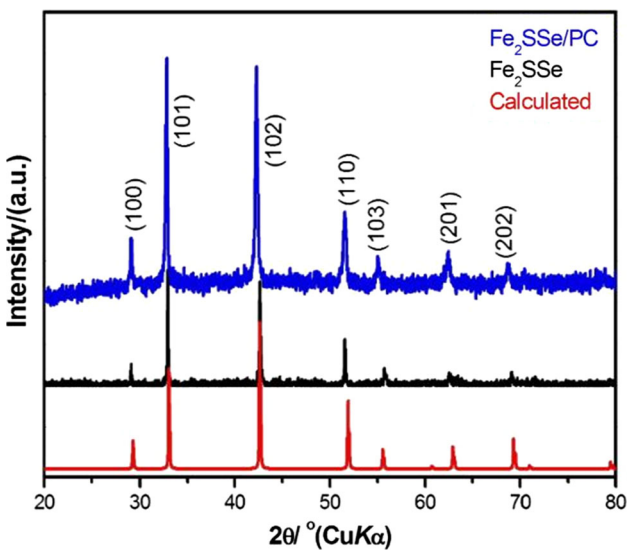

Figure 1 The powder XRD patterns of Fe_2SSe/PC (*blue*) and pure Fe_2SSe (*black*).

Results and discussion

Structure and morphology characterization

The content of Fe_2SSe in Fe_2SSe/PC was determined by heating the sample in the air and calculating the weight of Fe_2O_3, which is about 88 %.

As seen in Fig. 1, the main PXRD peaks of Fe_2SSe/PC and pure Fe_2SSe were located at 29.8°, 33.04°, 42.6°, 51.9°, 55.56°, 62.92°, and 69.52°, corresponding to the calculated ones, indicating the obtained samples were pure Fe_2SSe/PC and Fe_2SSe. Energy-dispersive X-ray spectroscopy elemental analysis of Fe_2SSe/PC shows that C, Fe, S, and Se exist and the ratio of Fe, Se, and S is around 2:1:1 (Fig. 2a). The EDS element mapping analysis (Fig. 2b) of Fe_2SSe/PC indicates that Fe, S, Se, and N are evenly distributed on the surface of carbon [24–27].

Figure 3 shows the Raman spectrum of Fe_2SSe/PC. Two peaks appear at 1348.79 and 1589.62 cm^{-1}, which are caused by the effects of defects (D) and graphitization (G), respectively [27]. Furthermore, the intensity of D band is much higher than that of G band, indicating that there are some defects and interspaces on the surface of the carbon.

Figure 4 shows the X-ray photoelectron spectroscopy (XPS) spectrum which is used to analyze the chemical composition and valence of Fe_2SSe/PC. The smooth C 1*s* spectrum (Fig. 4a) shows four peaks at 284.78, 284.80, 285.88, and 287.28 eV, indicating that

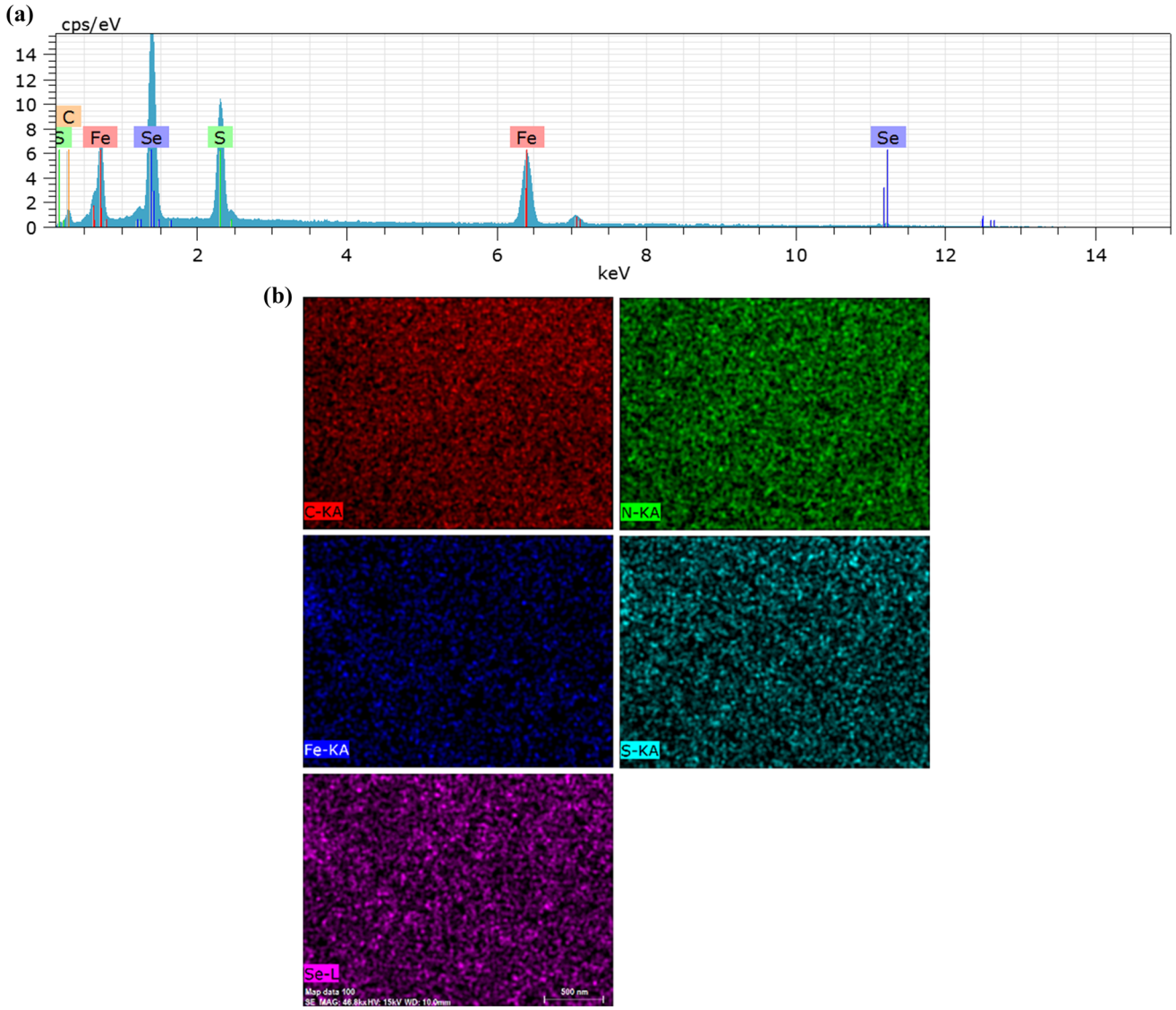

Figure 2 Energy-dispersive X-ray spectroscopy analysis (**a**) and elemental mapping images (**b**) for Fe_2SSe/PC.

there are a large number of C=C, C–C, C–N, and C=N bonds, respectively [28]. The Fe 2*p* (Fig. 4b) spectrum has two strong peaks at 710.78 and 724.98 eV, which are consistent with those of Fe^{2+}. Furthermore, the characteristic peaks of S^{2-} appear at 161.78 and 163.18 eV from the S 2*p* spectrum (Fig. 4c). The Se 3*d* (Fig. 4d) spectrum shows two peaks at 54.08 and 55.88 eV, which approve that Se is in form of negative bivalent in the composite [21, 29]. All these XPS peaks indicate that the as-prepared sample is really Fe_2SSe and carbon with abundant single and double bonds, corresponding to the results of PXRD, EDS, and Raman spectrum.

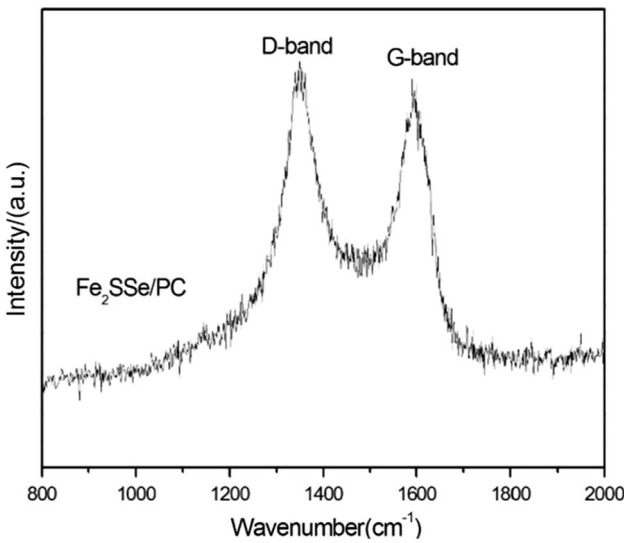

Figure 3 Raman spectrum of Fe_2SSe/PC.

Figure 5 shows the SEM images of Fe_2SSe/PC, pure CPAN (carbon form the carbonization of PAN), and pure Fe_2SSe. Compared with pure Fe_2SSe, the Fe_2SSe particles in Fe_2SSe/PC (Fig. 5c) have much smaller sizes with around hundreds of nanometers, which are partially inserted to the pores on the surface of CPAN. It can be observed that the Fe_2SSe particles in Fe_2SSe/PC have smaller sizes than those of pure ones, so the specific surface area of Fe_2SSe in Fe_2SSe/PC is larger than that of pure Fe_2SSe, which can expand the area of effective interaction between the active materials and electrolyte. What is more, smaller size is beneficial to shorten the Li^+ diffusion

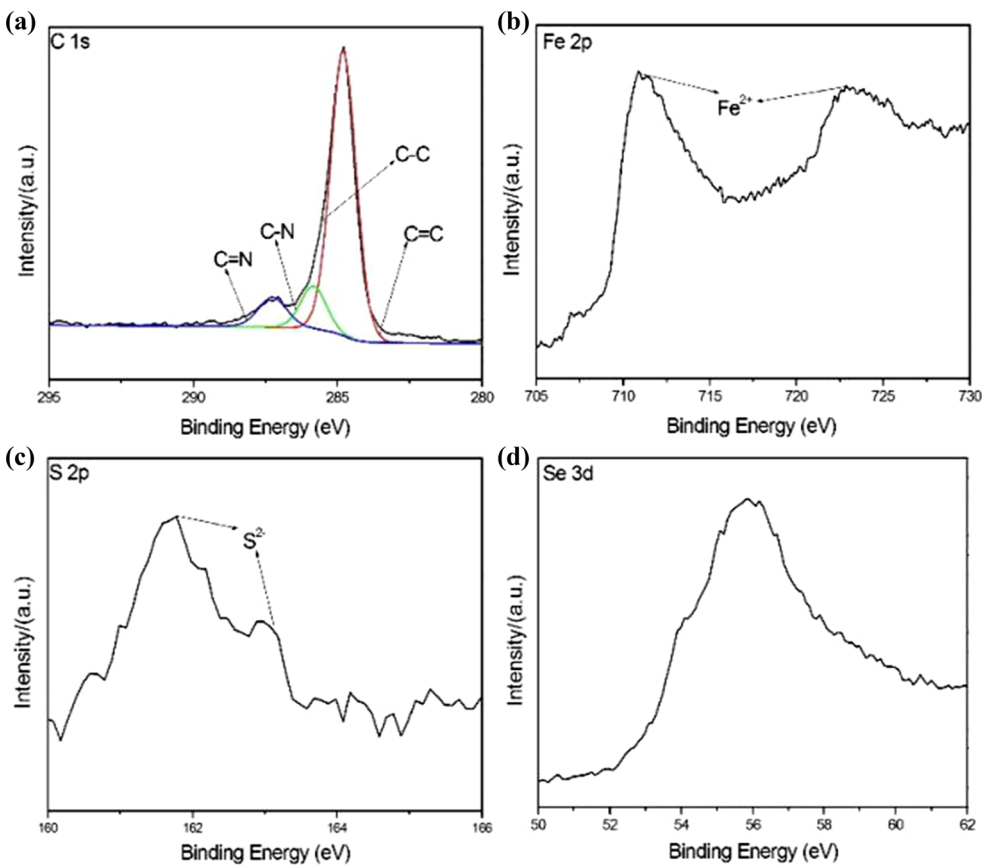

Figure 4 XPS spectra of Fe_2SSe/PC: **a** C 1*s*; **b** Fe 2*p*; **c** S 2*p*; **d** Se 3*d*.

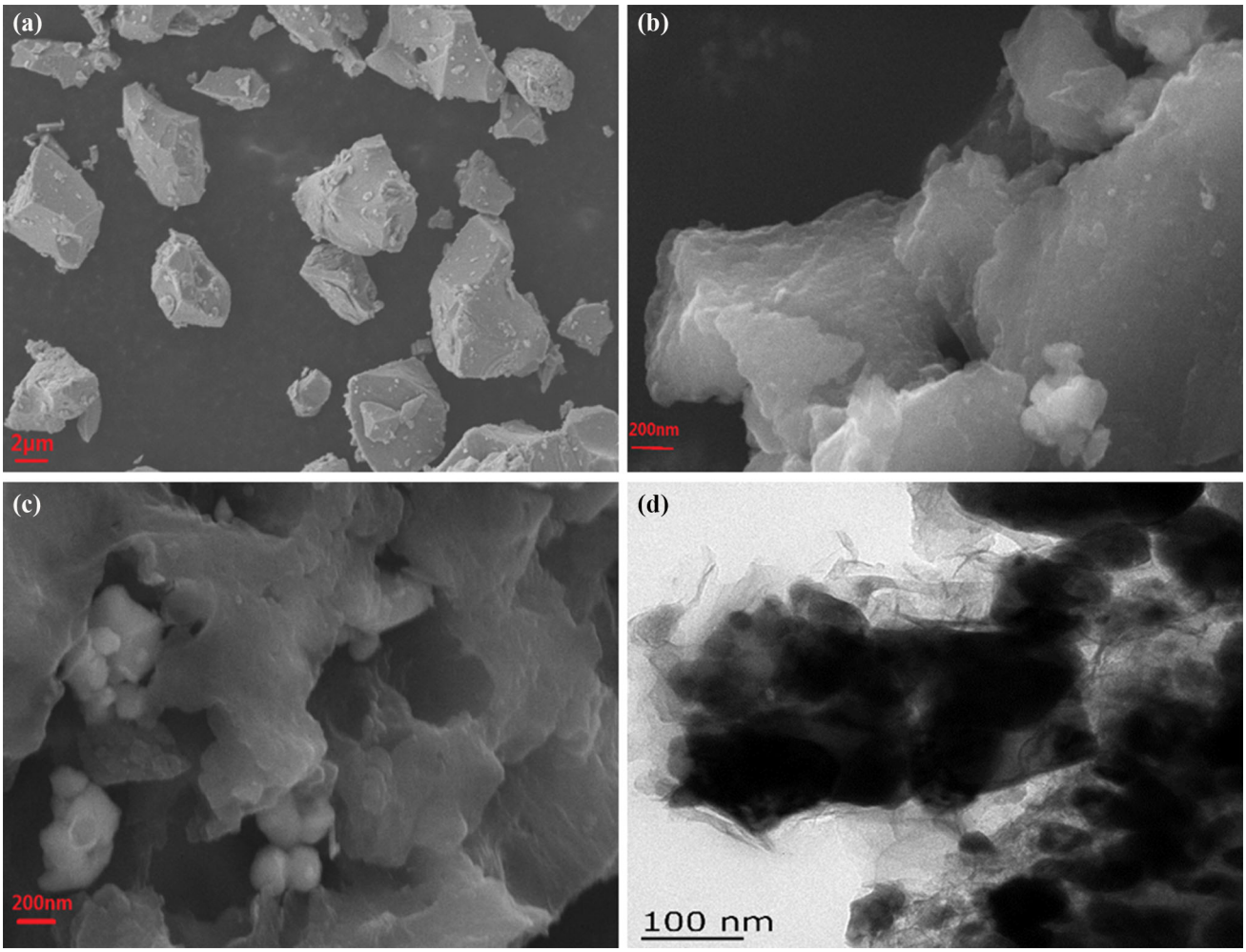

Figure 5 The SEM images of pure Fe_2SSe (**a**), pure CPAN (**b**), and Fe_2SSe/PC (**c**); the TEM image of Fe_2SSe/PC (**d**).

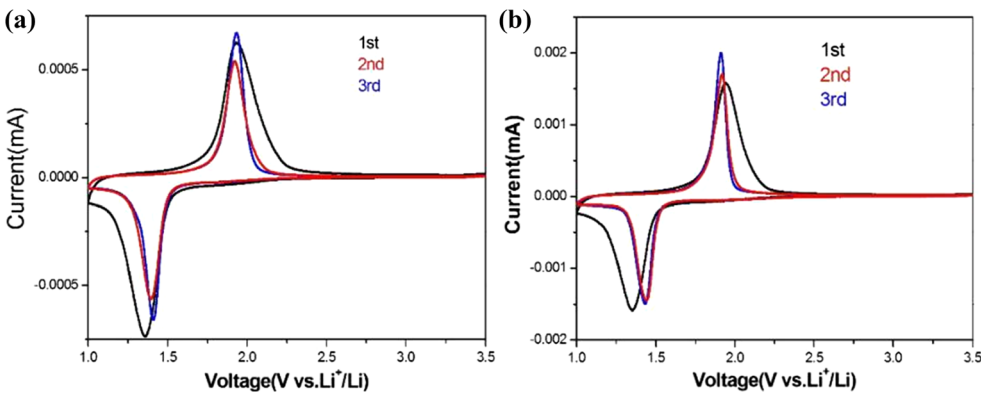

Figure 6 Cyclic voltammograms of pure Fe_2SSe (**a**) and Fe_2SSe/PC (**b**) for the first three cycles.

route and enhances the kinetics of charge carrier transport [14]. The TEM image (Fig. 5d) further shows that the Fe_2SSe particles are wrapped in the carbon, which is well consistent with the results of the SEM images.

Electrochemical performance

The redox reaction occurred on the electrode was studied using cyclic voltammetry (*C*–*V*) measurement. Figure 6a, b show the test results for pure Fe_2SSe and

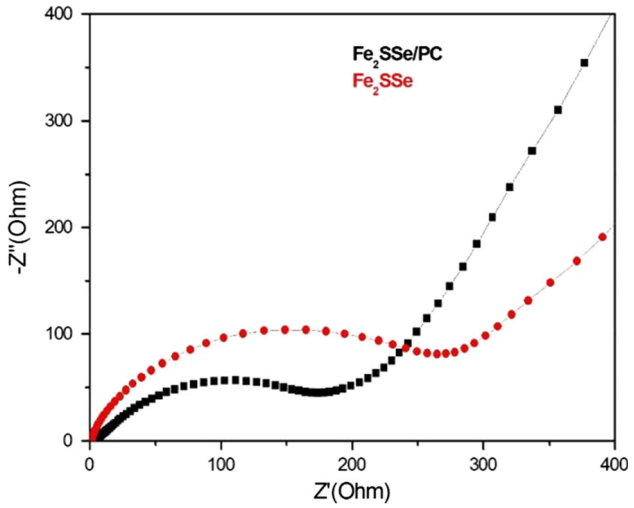

Figure 7 Nyquist plots for Fe_2SSe/PC (*black*) and pure Fe_2SSe (*red*) for the freshly assembled cells in the frequency range from 100 to 0.01 Hz.

Fe_2SSe/PC for the first three cycles, respectively. Both of the *C–V* curves are similar. For pure Fe_2SSe (Fig. 6a), a reduction peak is located at 1.36 V on the first loop, which could be described as follows [23]:

$$Fe_2SSe + 4Li^+ + 4e^- \rightarrow Li_2S + 2Fe + Li_2Se. \quad (1)$$

The broad oxidation peak appearing at 1.93 V indicates that Fe_2SSe phase formed again. After the first cycle, the location of the reduction peak was at 1.43 V and stable. The oxidation peaks were located at 1.93 V all the time, which can be explained using the following reaction [23, 30].

$$Li_2S + 2Fe + Li_2Se \rightarrow Fe_2SSe + 4Li^+ + 4e^-. \quad (2)$$

Electrochemical impedance spectroscopies of pure Fe_2SSe and Fe_2SSe/PC were investigated to know

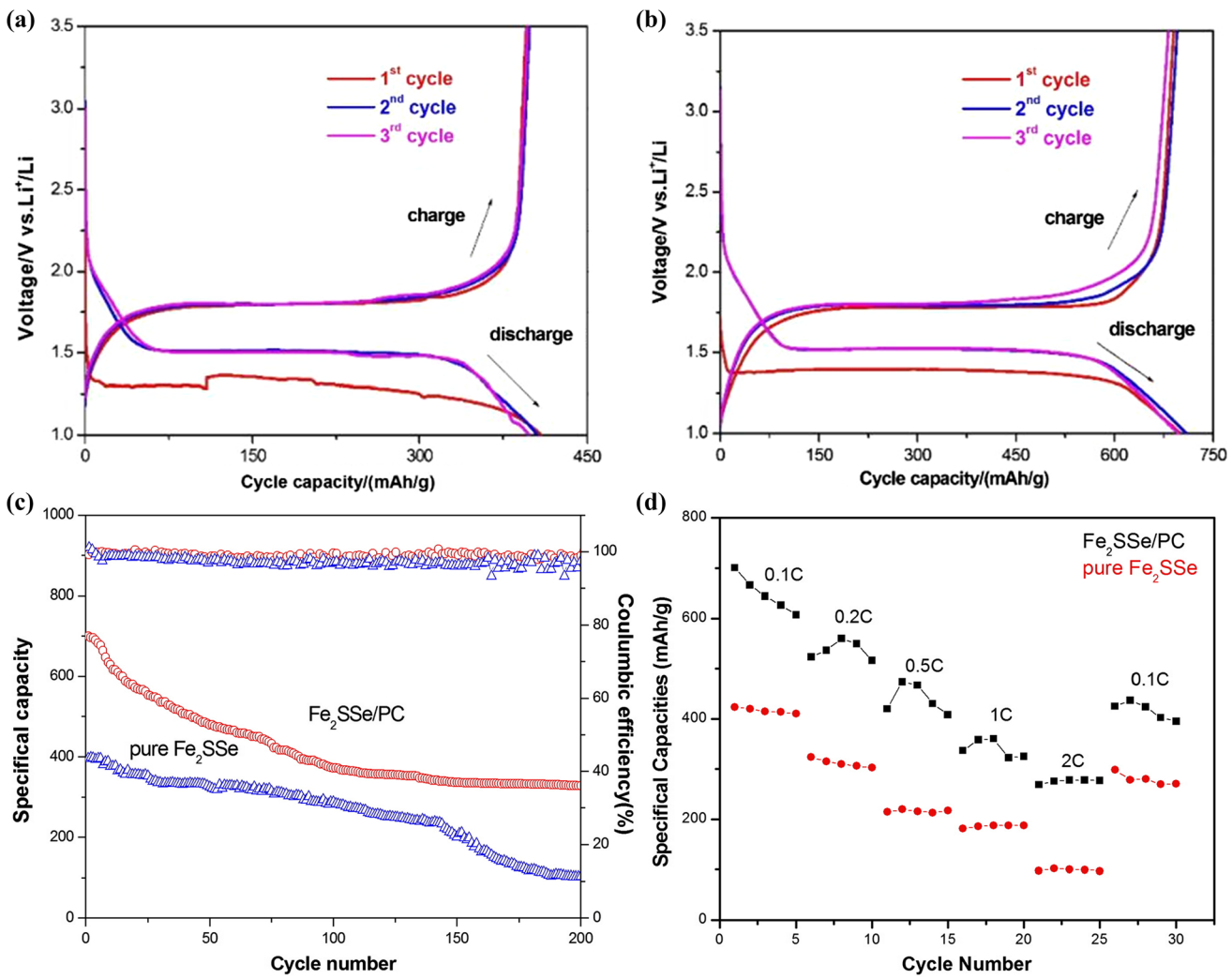

Figure 8 Charge and discharge curves of Fe_2SSe/PC **a** and pure Fe_2SSe **b** electrodes during the initial 3th cycles; **c** Cyclic stability of Fe_2SSe/PC and pure Fe_2SSe electrodes for 200 cycles at 0.1 C; **d** Rate capabilities of Fe_2SSe/PC and pure Fe_2SSe at various current densities.

more about the interface performance of electrode materials in Fig. 7. Both of the impedance curves consist of a semicircle set in high frequency and a straight line of low-frequency region, which reflect the charge transfer resistance at the interface of the electrode and the electrolyte, and ion diffusion resistance in the electrolyte, respectively. It is obvious that the radius of the semicircle for the Fe_2SSe/PC is much smaller than that of pure Fe_2SSe in the high frequency, indicating a lower resistance. This as well proves that CPAN plays an important role for the enhancement of Fe_2SSe/PC's electrical conductivity.

The cyclic performance of the electrode material for pure Fe_2SSe (Fig. 8a) and Fe_2SSe/PC (Fig. 8b) was evaluated between 1.0 and 3.5 V at 0.1 C. Obviously, the initial discharge capacity of pure Fe_2SSe was only 395.3 mAh/g. On the contrary, Fe_2SSe/PC electrode prepared at the same conditions could deliver about two times initial capacity of 699.5 mAh/g than that of pure Fe_2SSe. The capacity enhancement is most probably ascribed to stabilized PAN matrix, which can effectively prevent active material loss and bear the volume changes during Li^+ insertion/extraction process [31]. Besides, Fe_2SSe/PC could still remain the capacity of 327.9 mAh/g after 200 cycles, which is much higher than the capacity of 102.3 mAh/g for the pure Fe_2SSe electrode (Fig. 8c). Furthermore, Fe_2SSe/PC displays a good Coulomb efficiency, which is maintained above 99 % during the charge and discharge for 200 cycles.

The rate capabilities of Fe_2SSe/PC and pure Fe_2SSe were also performed (Fig. 8d). Obviously, the specific capacities were decreased along with the increase of the discharge/charge rates from 0.1 to 2 C. The third cycle discharge capacities of Fe_2SSe/PC reach around 643.8, 560.5, 466.9, 360.6, and 277.6 mAh/g at 0.1, 0.2, 0.5, 1 and 2 C, respectively. The discharge capacity of 423.7 mAh/g can be still left when the current density comes back to 0.1 C, indicating that the Fe_2SSe/PC has a better reversibility and rate capacity than that of pure Fe_2SSe. These results reveal that the incorporation of CPAN into pure Fe_2SSe can effectively enhance its electrochemical performance.

Conclusions

The Fe_2SSe/PC was successfully prepared using a simple one-pot solid-state method. It exhibits an initial discharge capacity of 699.5 mAh/g at 0.1 C and 327.9 mAh/g can be still maintained after 200 cycles when it is used as the anode material for LIBs. In our opinions, this method can be also used to prepare other M_2SSe@PC (M: transition metal) composites.

Acknowledgements

We gratefully acknowledge the financial support by the Higher Education Science Foundation of Jiangsu Province (No. 15KJB150031), State Key Laboratory of Structural Chemistry Fund (No. 20150009), the Qing Lan project, and the Priority Academic Program Development of Jiangsu Higher Education Institutions. We would also like to acknowledge the technical support received from the Testing Center of Yangzhou University.

References

[1] Liu X, Zhang K, Lei KX, Li FJ, Tao ZL, Chen J (2016) Facile synthesis and electrochemical sodium storage of CoS_2 micro/nano-structures. Nano Res 9:198–206

[2] Douglas A, Carter R, Oakes L, Share K, Cohn AP, Pint CL (2015) Ultrafine iron pyrite (FeS_2) nanocrystals improve sodium-sulfur and lithium–sulfur conversion reactions for efficient batteries. ACS Nano 9:11156–11165

[3] Zeng ZY, Zhang XW, Bustillo K, Niu KY, Gammer C, Xu J, Zheng HM (2015) In situ study of lithiation and delithiation of MoS_2 nanosheets using electrochemical liquid cell transmission electron microscopy. Nano Lett 15:5214–5220

[4] Xiong FY, Cai ZY, Qu LB, Zhang PF, Yuan ZF, Asare OK, Xu WW, Lin C, Mai LQ (2015) Three-dimensional crumpled reduced graphene oxide/MoS_2 nanoflowers: a stable anode for lithium-ion batteries. ACS Appl Mater 7:12625–12630

[5] Tarascon JM, Armand M (2001) Issues and challenges facing rechargeable lithium batteries. Nature 414:359–367

[6] Jiang H, Ge YQ, Fu K, Lu Y, Chen C, Zhu JD, Dirican M, Zhang XW (2015) Centrifugally-spun tin-containing carbon nanofibers as anode material for lithium-ion batteries. J Mater Sci 50:1094–1102. doi:10.1007/s10853-014-8666-5

[7] Xia L, Qiu KH, Gao YY, He X, Zhou FD (2015) High potential performance of Cerium-doped $LiNi_{0.5}Co_{0.2}Mn_{0.3}O_2$ cathode material for Li-ion battery. J Mater Sci 50:2914–2920. doi:10.1007/s10853-015-8856-9

[8] Zhang PG, Zhang CY, Xie AJ, Li C, Song JM, Shen YH (2016) Novel template-free synthesis of hollow@porous TiO_2 superior anode materials for lithium ion battery. J Mater Sci 51:3448–3453. doi:10.1007/s10853-015-9662-0.pdf

[9] Deng TS, Zhou XP (2016) Porous graphite prepared by molybdenum oxide catalyzed gasification as anode material for lithium ion batteries. Mater Lett 176:151–154

[10] Wu GH, Li RY, Liu JK, Gu ZG, Wang GL (2015) N-doped graphene/graphite composite as a conductive agent-free anode material for lithium ion batteries with greatly enhanced electrochemical performance. Electrochim Acta 171:156–164

[11] Ji JY, Liu JL, Lai LF, Zhao X, Zhen YD, Lin JY, Zhu YW, Ji HX, Zhang LL, Ruoff RS (2015) In situ activation of nitrogen-doped graphene anchored on graphite foam for a high-capacity anode. ACS Nano 9:8609–8616

[12] Zhao L, Yu XQ, Yu JZ, Zhou YG, Ehrlich SN, Hu YS, Su D, Li H, Yang XQ, Chen LQ (2014) Remarkably improved electrode performance of bulk MnS by forming a solid solution with FeS-understanding the Li storage mechanism. Adv Funct Mater 24:5557–5566

[13] Guo SP, Li CX, Chi Y, Ma Z, Xue HG (2016) Novel 3-D network SeS_x/NCPAN composites prepared by one-pot in situ solid-state method and its electrochemical performance as cathode material for lithium-ion battery. J Alloys Compd 664:92–98

[14] Xu C, Zeng Y, Rui XH, Xiao N, Zhu JX, Zhang WY, Chen J, Liu WL, Tan HT, Hng HH, Yan QY (2012) Controlled soft-template synthesis of ultrathin C@FeS nanosheets with high-Li-storage performance. ACS Nano 6:4713–4721

[15] Fei L, Williams BP, Yoo SH, Carlin JM, Joo YL (2016) A general approach to fabricate free-standing metal sulfide@-carbon nanofiber networks as lithium ion battery anodes. Chem Commun 52:1501–1504

[16] Fei L, Lin QL, Yuan B, Chen G, Xie P, Li YL, Xu Y, Deng SD, Smirnov S, Luo HM (2013) Reduced graphene oxide wrapped fes nanocomposite for lithium-ion battery anode with improved performance. ACS Appl Mater 5:5330–5335

[17] Xing CC, Zhang D, Cao K, Zhao SM, Wang X, Qin HY, Liu JB, Jiang YZ, Meng L (2015) In situ growth of FeS microsheet networks with enhanced electrochemical performance for lithium-ion batteries. J Mater Chem A 3:8742–8749

[18] Zhu CB, Wen YR, Yu Y (2015) High lithium storage performance of FeS nanodots in porous graphitic carbon nanowires. Adv Funct Mater 25:2335–2342

[19] Chen GY, Sun Q, Yue JL, Shadike L, Yang Y, Ding F, Sang L, Fu ZW (2015) Conversion and displacement reaction types of transition metal compounds for sodium ion battery. J Power Sour 284:115–121

[20] Zhang K, Hu Z, Liu X, Tao ZL, Chen J (2015) $FeSe_2$ microspheres as a high-performance anode material for Na-ion batteries. Adv Mater 27:3305–3309

[21] Huang SS, He QQ, Chen WL, Zai JT, Qiao QQ, Qian XF (2015) 3D hierarchical $FeSe_2$ microspheres: controlled synthesis and applications in dye-sensitized solar cells. Nano Energy 15:205–215

[22] Chen D, Wang XS, Chen JT, Ren Z, Xue MQ, Chen GF (2015) Rewriting the superconductivity in iron-based superconductors by lithium-ion insertion and extraction. Adv Mater 27:4224–4228

[23] Liu JB, Yang Y, Liu XJ, Xue MZ, Liu JS, Cui YH (2016) Facile synthesis and electrochemical properties of Fe_2SeS for lithium ion batteries. J Power Sour 306:317–321

[24] Tang J, Liu J, Li CL, Li YQ, Tade MO, Dai S, Yamauchi Y (2015) Synthesis of nitrogen-doped mesoporous carbon spheres with extra-large pores through assembly of diblock copolymer micelles. Angew Chem Int Ed 54:588–593

[25] Li L, Wang CL, Liao JY, Manthiram A (2015) Dual-template synthesis of N-doped macro/mesoporous carbon with an open-pore structure as a metal-free catalyst for dye-sensitized solar cells. J Power Sour 300:254–260

[26] Liang HW, Wu ZY, Chen LF, Li C, Yu SH (2015) Bacterial cellulose derived nitrogen-doped carbon nanofiber aerogel: an efficient metal-free oxygen reduction electrocatalyst for zinc-air battery. Nano Energy 11:366–376

[27] Ren YP, Lv WM, Wen FS, Xiang JY, Liu ZY (2016) Microwave synthesis of SnS_2 nanoflakes anchored graphene foam for flexible lithium-ion battery anodes with long cycling life. Mater Lett 174:24–27

[28] Liu YC, Zhang N, Yu CM, Jiao LF, Chen J (2016) $MnFe_2O_4$@C nanofibers as high-performance anode for sodium-ion batteries. Nano Lett 16:3321–3328

[29] Kong DS, Wang HT, Lu ZY, Cui Y (2014) $CoSe_2$ nanoparticles grown on carbon fiber paper: an efficient and stable electrocatalyst for hydrogen evolution reaction. J Am Chem Soc 136:4897–4900

[30] Kitajou A, Yamaguchi J, Hara S, Okada S (2014) Discharge/charge reaction mechanism of a pyrite-type FeS_2 cathode for sodium secondary batteries. J Power Sour 247:391–395

[31] Liu J, Wen Y, Wang Y, van Aken PA, Maier J, Yu Y (2014) Carbon-encapsulated pyrite as stable and earth-abundant high energy cathode material for rechargeable lithium batteries. Adv Mater 26:6025–6030